RSC Advances

ROYAL SOCIETY OF CHEMISTRY

www.rsc.org/advances

Effect of Mn doping on structural, morphological and dielectric properties of $EuFeO_3$ ceramics

Khalid Sultan[1*], M. Ikram[1] and K.Asokan[2]

[1]*Department of Physics, National Institute of Technology, Hazratbal Srinagar, J & K-190006, India.*

[2]*Materials Science Division, Inter University Accelerator Centre, Aruna Asaf Ali Marg, New Delhi-110067, India.*

Abstract

Polycrystalline compounds of $EuFe_{1-x}Mn_xO_3$ (x = 0.0, 0.3, 0.5) were synthesized by standard solid state reaction technique. These compounds were characterized by X-ray diffraction (XRD), Raman spectroscopy, Scanning electron microscopy (SEM) and dielectric properties. The Rietveld analysis of the XRD profiles clearly indicated that these compounds are well fitted with orthorhombic structure and space group *Pbnm*. Raman spectral features revealed their finger print modes and irreducible representations at the Brillouin zone center as per the group theory. The surface morphologies from SEM images revealed that the average grain size increases with Mn doping. Energy dispersive x-ray analysis indicated the presence of Eu, Fe, Mn and oxygen. The dielectric properties were studied as a function of frequency and temperature. Absence of any loss peak in the dielectric dispersion suggests its behaviour to be that of quasi-dc-process (QDC). The increase of dielectric constant with Mn doping suggests that small polarons contribute to the conduction mechanism.

Key Words: Ceramics, orthoferrites, dielectric properties, conduction mechanism.

*Corresponding author Tel.: +91-9419031528 *Email: ksbhat.phy@gmail.com

1. Introduction.

The orthoferrite $EuFeO_3$ crystallizes in the orthorhombic perovskite structure in which the FeO_6 octahedra are distorted and the extent of distortion depends on the ionic size of the rare earth ion, Eu and oxygen stiochiometry. The compounds crystallize in the space group *Pbnm* with four distorted perovskite units in the true crystallographic orthorhombic cell [1–7] where Eu^{3+} and the transition metal ions occupy the dodecahedral A and octahedral B-sites respectively. In this structure, the distortion of rare earth (Eu) polyhedra is large. The 12 (twelve) O ions surrounding the rare earth 'Eu' separate into two types: Eu with eight first-nearest O ions and Eu with four second-nearest O ions. Such structural distortions influence the magnetic ordering and spin-state transitions [8]. The crystallographic unit cell of $EuFeO_3$ (Fe being in high spin state) can be visualized as a corner sharing FeO_6 octahedron forming a three dimensional distorted perovskite structure [9]. In general, the orthoferrites are anti-ferromagnetic (AF) due to the anti-parallel alignment of the magnetic moments of the Fe sublattices. In the case of heavy rare-earth orthoferrites, however, a weak ferromagnetism is present due to a small canting in the alignment of the antiferromagnetically coupled lattices. This small canting, which is of the order of 10^{-2} rad [10], is enough to produce a very small net magnetic moment in the range 0.04–0.05 μB $molecule^{-1}$ [11].

Polycrystalline $EuFeO_3$ (hereafter referred as, EFO) compounds are very good dielectric materials and have many technological applications ranging from microwave to radio frequencies and hence potential candidates in microelectronic industry due to the high dielectric constant (ε') and low dielectric loss (tanδ). Hence, it is important to study their dielectric behavior at different frequencies. The conductivity of ferrites is also very high, which is one of the major considerations for microwave applications. The order of magnitude of the conductivity

greatly influences the dielectric and magnetic behavior of ferrites. EFO exhibits remarkable electrical and magnetic properties due to mixed valency of Fe ions and also because of anion non-stoichiometry which is commonly found in these oxides [12-13]. Partial replacement of the cation Fe by several other elements such as Mn ions can tailor various physical properties such as dielectric behavior and can create new applications [14-17]. EFO is Jahn-Teller (JT) inactive. After replacing Fe with Mn, the compound $EuFe_{1-x}Mn_xO_3$ (EFMO) becomes JT-active because of Mn^{3+} ions. It is reported that the t_{2g}^3 e_g^1 state of Mn^{3+} is subjected to JT effect resulting in the distortion of MnO_6 octahedra with four Mn-O distances of 0.1930 nm and two of 0.2290 nm [18]. The substitution of Mn ions in EFO weakens the exchange interaction and reduces the Curie temperature. It also induces a J-T distortion which results in a large electric field gradient at the ^{57}Fe nucleus and modification of crystallographic structure.

Present study focuses on the effect of Mn doping on the structural, morphological and dielectric properties of EFMO and evaluate the parameters like lattice parameters, dielectric constants, a.c conductivity and activation energy. A possible conduction mechanism for these compounds is also discussed.

2. Experimental details

Polycrystalline compositions of $EuFe_{1-x}Mn_xO_3$ (x=0.0, 0.3, 0.5) were prepared by solid state reaction method by mixing the stoichiometric ratio of high purity of 99.99% powders of Eu_2O_3, Mn_2O_3 and Fe_2O_3. These mixed powders were preheated at 1000^0C for 12 hours and then calcinated again at 1200^0C for 12 hours. The chemical reaction, $Eu_2O_3 + Fe_2O_3 \rightarrow 2\ EuFeO_3$ takes place. The homogenous powder was reground and pellets of 10 mm in diameter were made by the application of 5 kN force. The resultant pellets were sintered at 1300^0C for 24 hours at a

heating rate of 4^0C min^{-1} and then cooled to room temperature at a cooling rate of 3^0C min^{-1} in a tubular furnace. The calcinated material was analyzed by X-ray diffraction (XRD) using Bruker D8 Advance diffractometer (Cu-Kα radiation). The diffraction angle (2θ) was scanned from 20-80^0 at room temperature at voltage 40 KV, current 40 mA, step size of 0.02 and scan speed of $0.5^{0/}$min. Raman spectra were recorded with a Labram-HR800 micro Raman spectrometer equipped with a Peltier cooled charge-coupled device detector using an Ar excitation source having a wavelength of 488nm. No melting or phase transition was observed in the sample at excitation of Laser power of 10 mW. The SEM micrographs and energy dispersive analysis of X-rays (EDAX) analysis were obtained using an energy dispersive spectrometer (OXFORD ISIS-300 system) attached to a scanning electron microscope JEOL JSM-6490LV. The dielectric properties were measured using Agilent 4285A precision LCR meter and Lakeshore temperature controller as a function of frequency of the applied ac field in the range of 20 Hz to 2 MHz and at temperature ranging from 80 K to 400 K.

3. Results and discussions

3.1 XRD Analysis

X-ray diffraction studies were performed to study the phase purity of compounds of $EuFe_{1-x}Mn_xO_3$ (x = 0, 0.3 and 0.5). The XRD data of all these samples were analyzed using Rietveld refinement fullprof code [19]. Figure 1 shows XRD patterns of $EuFe_{1-x}Mn_xO_3$(a) x = 0.0, (b) x = 0.3 and (c) x = 0.5 along with the fitted graphs and the difference line. This clearly indicates that the XRD patterns are well fitted with space group *Pbnm*. $EuFeO_3$ crystallizes into $GdFeO_3$ orthorhombic Pbnm structure with Eu at wyckoff position (4c) (x y 1/4), Fe/Mn having position 4b (1/2 0 0) and O_2 is at 8d (x y z). The calculated parameters, Rwp, Rexp and goodness of fitting factors are shown in table I. The lattice constants a, b and c were determined from the

refinement program and are shown as a function of Mn content. The small change in lattice parameters and almost no change in cell volume with Mn substitution confirm that Mn^{3+} has almost similar ionic radii to that of $Fe^{3+}$and is substituted at the Fe^{3+}sites. From the XRD results, the samples with Mn concentrations up to x = 0.5 are in single phase having an orthorhombic structure and space group *Pbnm*. The lattice constants 'a' and 'c' decreases with Mn content while the lattice constant 'b' increases with Mn content. From the table, it is clear that within the doping range x=0.5, the lattice parameter $c/\sqrt{2} > a$. With increasing Mn, the lattice parameters a and $c/\sqrt{2}$ decrease but the change in former is less than later. It was observed that the compound $EuFe_{1-x}Mn_xO_3$ exhibits O-type ($a < c/\sqrt{2} < b$) orthorhombic *pbnm* structure which is commonly observed in all ABO_3 perovskite compounds [20-21].

3.2 Morphological studies and Elemental analysis

A typical SEM images of Mn doped $EuFeO_3$ sintered at 1300^0C for 24 h are shown in Fig. 2. The microstructure reveals that the particles are irregular in shape with varying sizes. The size of the grains vary from 2μm to 6 μm, and it is found that the average grain size is modified with Mn doping, also it is seen that the porosity decreases with Mn doping which may result in increase in the values of dielectric constant (as observed in dielectric data). It is believed that BO_6 octahedra are not rigid due to oxygen non- stoichiometry. Any strain or pressure at B sites may lead to in-phase or out-of phase tilting of BO_6. In addition, Mn occupies the iron site of FeO_6 octahedra, thus leading to the change of bond angle and bond length and Fe-O binding energy will decrease which is favorable for the formation of more oxygen vacancy traps on the surface. In addition to this it is also observed from Table I that the lattice parameters as well as cell volume decreases with Mn doping resulting in the formation of smaller grains. The smaller grains fit well and lead to decrease in porosity and consequently densification occurs in the

compound with Mn doping. EDAX spectra of EFMO compounds are also shown in Fig. 2. The presence of Eu, Fe, Mn and O ions are clearly seen in the spectra. Due to overlapping of energies of Fe, Mn and Eu ions, quantitative estimation of these ions were not reliable.

3.3 Raman study

Raman signature of perovskite structure arises from the two interpenetrated lattices: the covalent entities constituting the structure (BO_6 octahedron sharing common oxygen ions) and the second one made of highly Columbic ions. These contribute to the translation oscillation modes which couple themselves with other vibrational modes of the neighboring entities: translations and rotations/vibration of iono-covalent BO_6 entity leading to the wave number shifts. The Raman spectra of $EuFe_{1-x}Mn_xO_3$ (x = 0, 0.3 and 0.5) compounds at room temperature (300 K) is shown in Fig.3 with inset showing shifting of B_{1g} mode to higher wave number region with doping.

One of the interesting characteristic of Raman scattering is sensitivity to strain in the sample [22]. When the material is under strain, its Raman wave will deform/shift from the original status and in that case this mechanical quantity is possible to be directly measured. It is now an established fact that compressive stress results in the shift of the position of the Raman peak towards higher wave number region (commonly called “Blue shift”), while tensile stress results in a shift towards lower wave number (“Red shift”) [23]. In this study it is clear from Fig.3 that the modes exhibit a blue shift (hardening behavior) with broadening of FWHM’s in the doped samples which may arise due to the chemical pressure developed in the sample after the inclusion of JT-active Mn^{3+} ions. The Raman spectra show that there is a disorder in the vibrational bands with increasing Mn content, which is primarily obvious because most of the

Raman modes below 600 cm^{-1} are suppressed by the substitution of Mn ions (x =0.3 and 0.5) and the only mode visible throughout the series is the B1g/J-T mode (near 624 cm^{-1} in pristine sample). In perovskites containing trivalent Fe and Mn, the energy of crystal field splitting is smaller than the Hund's energy between two electrons [24-25]. So the Fe and Mn ions are in the high spin state. The trivalent Fe and Mn ions with high spin state have electronic configurations as follows: Fe^{3+}: t_{2g} ($d_{xy}\uparrow$, $d_{yz}\uparrow$, $d_{xy}\uparrow$), e_g ($d_{(x^2-y^2)}\uparrow$, $d_{z^2}\uparrow$) and Mn^{3+} : t_{2g} ($d_{xy}\uparrow$, $d_{yz}\uparrow$, $d_{xy}\uparrow$), e_g ($d_{(x^2-y^2)}\uparrow$, d_{z^2}). Mn^{3+} has a $3d^4$ configuration and exhibits JT distortion. The observed shift in wave number with doping clearly indicates the change in Fe-O / Mn-O bond lengths as well as impact on FeO_6 / MnO_6 octahedra.

3.4 Dielectric Studies

(a) Dependence of dielectric behavior on frequency

The variation of dielectric constant as a function of frequency at different temperatures for Mn doped EFO compounds are shown in fig 4(i). The value of dielectric constant decreases continuously with frequency for all the three compositions (x=0, 0.3 and 0.5) at all the measured temperatures. Similar behavior has been reported by many investigators [24-27] and can be explained on the basis of polarization mechanism. At low frequencies, all the mechanisms of polarization contribute to the dielectric constant and with the increase in frequency, the contributions from various types of polarizations starts decreasing. For example, at very high frequencies of the order of 10^{15} Hz, only electronic polarization contributes to the dielectric constant.The dielectric loss (tanδ) is a measure of lag in the polarization with respect to the applied alternating field. The variation of tanδ with frequency for different doping concentrations at 300 k is shown in Fig.4 (ii). The absence of any loss peak in the dielectric dispersion of the material (Fig.4 (ii)) suggests its behavior to be that of quasi-dc process (QDC) [28–31]. In QDC

process no loss peak is observed and the real and imaginary parts of susceptibility increase rapidly towards low frequencies without any sign of saturation and follow a parallel trend in a log–log representation and obey a power law of the type:

$$\chi \propto \omega^{n-1}; \quad 0 < n < 1$$

Where $\omega = 2\pi f$ is the measuring frequency and χ is the electric susceptibility of the material which is related to real dielectric constant as $\chi = \varepsilon' - 1$.

In case of material under study, n = 0.83, 0.85 and 0.89 for x = 0.0, 0.3 and 0.5 respectively which is obtained from the plot of log χ verses log ω (Fig. 5). The universal fractional power law is obeyed by a variety of solid materials, including low loss dielectrics, dipolar materials, hopping electronic systems, ionic conductors, semiconductors, p–n junctions, interfacial phenomena, and mechanical relaxation [31]. It should be noted that dipolar system exhibits loss peaks, whereas carrier-dominated systems exhibit QDC responses.

The conductivity representation is a most prominent representation to relate the macroscopic measurement to the microscopic movement of the ions. The a.c conductivity has been calculated from the real and imaginary parts of the impedance data measured over a study range of temperatures. Fig.6 presents the variation of log σ versus log ω (linear fitted) for different doping concentrations at room temperature (300 K). The frequency dependent conductivity displays a low frequency plateau and high frequency dispersive regions. The frequency independent conductivity characterizes the d.c. conductivity, due to the random diffusion of the ionic charge carriers via activated hopping. However, power-law dispersion indicates a non-random process wherein the ions perform correlated forward–backward motion. When the temperature increases, the transition from d.c. to the dispersive region shifts towards

the higher frequency range. The conductivity, $\sigma_{ac}(\omega)$, is analyzed using Jonscher's universal power law:

$$\sigma_{ac} = \sigma(0) + A\omega^s$$

Where σ (0) is the d.c conductivity and $\omega = 2\pi f$ is the measuring frequency. The frequency exponent 's' is related to the degree of correlation among moving ions and its value usually ranges between 0.6 and 1 for ion conducting materials. Non-zero '*s*' value in the dispersive region of conductivity is due to the energy stored in the short-range collective motion of ions. A higher '*s*' implies that large energy is stored in such collective motions. In the present case, s is calculated from the plot of log σ versus log ω at different composition (Fig. 6) and its values are 0.44, 0.385 and 0.301 for x = 0.0, 0.3 and 0.5 respectively.

(b) Dependence of dielectric behavior on temperature

The temperature dependence of dielectric constant (ε') and dielectric loss tangent (tan δ) at different frequencies for $EuFe_{1-x}Mn_xO_3$ (x = 0, 0.3 and 0.5) pellets is shown in Fig.7 and Fig. 8 respectively. The room temperature dielectric constant attains a value 330 for pure $EuFeO_3$. Two ε' plateaus at higher and low temperature are clearly seen [Fig. 7 a]. Between two plateaus, the dielectric constant increases sharply by a factor of approximately 100. At low temperatures the dielectric constant is almost independent of frequency and temperature. The step like increase in the dielectric constant indicates that there exists one thermally activated relaxation in EFO ceramic samples. At higher temperature due to generation of extra thermal energy the mobility of charge carriers increases and hence increases rate of hopping. At low temperatures, the thermal energy is not sufficient to contribute to the mobility of charge carriers. This observed mechanism sets up the higher polarization at higher temperature which increases the dielectric constant.

Figure 7 (d) shows variation of dielectric constant with temperature at 1 kHz for different Mn doping concentrations. With the increase in Mn doping dielectric behavior shows a general trend of increase in dielectric constant with increase in temperature. It is observed that the dielectric constant increases with Mn concentrations and attains a typically higher value at x =0.5. The possible explanation is related to the B-site in perovskite ferrites which plays a dominant role in the phenomena of electrical conductivity due to hopping of electrons in Cation $Fe^{3+} + e \leftrightarrow Fe^{2+}$ at B sites. Doping Mn ions in the compound $EuFeO_3$ induces chemical pressure. This results in Mn ions to be in mixed valence of trivalent and tetravalent states. To maintain the charge neutrality in the system Fe^{3+} gets converted into Fe^{2+}. The charge compensation equation involved may be written as,

$$Fe^{3+} + Mn^{3+} \leftrightarrow Fe^{2+} + Mn^{4+}$$

It thus Mn doping converts Fe^{3+} to Fe^{2+} and causes decrease in the resistance of grain thereby increasing the probability of electrons reaching the grain boundary. This becomes responsible for increase in polarization and hence the dielectric constant. Similar results were reported in Mn-substituted Ni-Zn ferrites by Amarendra et al. wherein the dielectric constant was shown to be sensitively controlled by Mn substitution [32].The variation of dielectric loss with temperature shows the same behavior as that of temperature vs. dielectric constant behavior.

The temperature dependent (at selected frequencies) ac conductivity plots for $EuFe_{1-x}Mn_xO_3$ (x = 0, 0.3 and 0.5) pellets respectively are shown in Fig. 9 respectively. A linear behavior is observed for ac conductivity with temperature for all frequencies at low temperature, and shows a sharp increase at higher temperature. This is attributed to the increase in the number of charge carriers and their drifted mobility which are thermally activated. At higher doping concentrations (x = 0.5) ac conductivity increases by orders of magnitude which can again be

attributed to hopping of Mn^{3+} to Mn^{4+} and Fe^{3+} to Fe^{2+}. The ac conductivity increases with frequency and the obtained results are in good agreement with the literature [33-34]. The ac conductivity alteration identifies that the conduction mechanism is following the charge hopping between localized states. The observed results follow small polaron conduction and are consistent with the literature [35-36]. The hopping frequency of charge carriers seems to be the function of the frequency of the applied field which results in increase in mobility of charge carriers. Since the conductivity is not increased by charge carriers instead it increases because of mobility of these carriers, therefore at certain higher frequency the hopping of charge carriers ceases to follow the applied field frequency and reduction in conductivity.

Activation energy (E_a) was calculated from the slope of the curve $\log\sigma_{ac}$ vs 1000/T (K^{-1}) using relation $\sigma = \sigma_0 e^{Ea/KT}$, where σ_0 the conductivity at infinite temperature and k is is is the Boltzmann's constant. The values of E_a for different doping concentrations are given in Table I. It is seen that the value of activation energy decreases with Mn doping in the compound $EuFeO_3$. The calculated value of E_a for the pristine compound $EuFeO_3$ which was 0.23 eV was slightly smaller than calculated by Bandi et al. [37] for $PrFeO_3$ which was about 0.32 eV. The possible reason can be different electronic structure of Pr and Eu as well as due to different preparation method of the samples.

Conclusion

Polycrystalline compounds of Mn doped $EuFeO_3$ were synthesized by solid state reaction method and the XRD analysis confirmed the orthorhombic structure with space group *Pbnm*. The SEM images of EFMO reveal that the particles are irregular in shape with average particle size of 2 μm to 6μm and average grain size increases with the Mn doping. The dielectric properties of EFMO compounds have strong dependence on both temperature and frequency of the applied

electric field. The absence of any loss peak in the dielectric dispersion of the material suggests its behavior to be that of quasi-dc process (QDC). The conductivity measurement shows that EFMO obeys Jonscher's universal power law. The ac conductivity variation shows that the conduction mechanism follows the charge hopping between localized states and follows the small polaron conduction. The present investigation clearly indicates that the physical properties of Mn doped EFO depend on the amount of doping and consequently on the charge state occupied by Fe and Mn ions.

Acknowledgements

Authors (K.S, and M.I) would like to thank the Director, IUAC, New Delhi for necessary experimental facilities and Director NIT Srinagar for encouragement in this research work.

References

[1]. Jia Liu, Wen-Qiang Cao, Hai-Bo Jin, Jie Yuan, De-Qing Zhang and Mao-Sheng Cao, ***J. Mater. Chem. C***, 2015,**3**, 4670-4677.

[2]. Ming-Ming Lu, Wen-Qiang Cao, Hong-Long Shi, Xiao-Yong Fang, Jian Yang, Zhi-Ling Hou, Hai-Bo Jin, Wen-Zhong Wang, Jie Yuan and Mao-Sheng Cao ***J. Mater. Chem. A***, 2014, **2**, 10540-10547.

[3]. Bo Wen, Mao-Sheng Cao , Zhi-Ling Hou, Wei-Li Song, Lu Zhang, Ming-Ming Lu, Hai-Bo JinXiao-Yong Fang, Wen-Zhong Wang, Jie Yuan, **Carbon**, 2013, **65**, 124-139.

[4] H.M Widatallah, A.H Harthi, C Johnson, Z Klencsar, A.M Gismelseed, E.A Moore Formation, cationic site exchange and surface structure of mechanosynthesized $EuCrO_3$ nanocrystalline particles. J. Phys. D Appl. Phys. 44 (2011) 265403.

[5] X Niu, W Du, W Du Preparation, characterization and gas-sensing properties of rare earth mixed oxides ,Sens Actuat. B Chem. 99 (2004) 399.

[6]. K Tsushima, I Takemura, S Osaka Weak-ferromagnetism in EuCrO3 Solid. State Commun. 7 (1969) 71.

[7]. T.C Gibb Europium-151 Mössbauer spectra of some orthorhombic perovskites J. Chem. Soc. Dalton Trans. (1981) 2245

[8]. M Marezio, P.D Dernier Crystal structures and crystal chemistry of the RETiO3 perovskites, Mater. Res. Bull 6(1971) 23.

[9]. A.R Moodenbaugh, B Nielsen, S Sambasivan, DA Fischer, T Friessengg, S Aggarwal, R Ramesh , RL Peffter Hole-state density of La1-xSrx CoO3 δ(0<x<0.5) across the insulator/metal phase boundary. Phys. Rev. B 61 (2000) 5666.

[10]. K Ueda, H Tabata, T Kawai Artificial Control of Spin Order and Magnetic Properties in $LaCrO_3$–$LaFeO_3$ Superlattices. Jpn. J. Appl. Phys. 38 (1999) 6690

[11]. F.J Kahn, P.S Pershan, J.P Remeika Ultraviolet Magneto-Optical Properties of Single-Crystal Orthoferrites, Garnets, and Other Ferric Oxide Compounds. Phys. Rev. Lett. 186 (1969) 891.

[12]. S.V Trukhanov Investigation of stability of ordered manganites. JETP 101 (2005) 513

[13]. S.V Trukhanov, L.S Lobanovski, M.V Businsky, V.V Fedotova, I.O Troyanchuk, A.V Trunkhanov, V.A Ryzhov, H Szymczak, R Szymczak, M Baran Microstructure evolution and magnetoresistance of the A-site ordered Ba-doped manganites. J. Phys. Condens. Matter 17 (2005) 6495.

[14]. S.S Bashkirov, V.V Parfenov, I.A Latif, L.D Zaripova Mössbauer effect and electrical properties studies of SmFe< sub> x</sub> Mn< sub> 1− x</sub> O< sub> 3</sub>(< i> x</i>= 0.7, 0.8 and 0.9). Journal of Alloys and Compounds 387 (2005) 70-73.

[15]. Y Nagata, S Yashiro, T Mitsuhashi, A Koriyama, Y Kawashima, H Samata Magnetic properties of RFe1−xMnxO3 (R=Pr, Gd, Dy) ,Journal of Magnetism and Magnetic Materials. 237 (2001) 250-260.

[16]. P. Porta, S. Cimino, S.D. Rossi, M. Faticanti, G. Minelli, $AFeO_3$ (A=La, Nd, Sm) and $LaFe_{1-x}Mg_xO_3$ perovskites Structural and redox properties. Materials Chemistry and Physics, 71 (2001) 165-173.

[17]. K. Sultan, M. Ikram, K. Asokan, Structural, optical and dielectric study of Mn doped $PrFeO_3$ ceramics. Vacuum 99(2014) 251-258.

[18]. R. Norrestam, α-Manganese(III)oxide—a C-type sesquioxide of ortho- rhombic symmetry. Acta Chem. Scand. 21 (1967) 2871

[19]. J.R. Carvajal, Recent Advances in Magnetic Structure Determination by Neutron Powder Diffraction. Physica B 192 (1993) 55-69.

[20]. J.A. Alonso, M.J. Martinez-lope, M.T. Casais, Evolution of the Jahn−Teller Distortion of MnO_6 Octahedra in $RMnO_3$ perovskites (R = Pr, Nd, Dy, Tb, Ho, Er, Y): A Neutron Diffraction Study. Inorg. Chem. 39 (2000) 917-923.

[21]. L. Li, X. Song, W. Su, Q. Wei, Z. Kang, The influence of substitution of Mn ions on quadrupole splitting of $EuFeO_3$ perovskite oxide. Hyperfine Interactions. 116 (1998) 167-172

[22]. E. Anastassakis, A. Canterero, M. Cardona, Piezo –Raman measurements and anhormonic parameters in silicon and diamond. Phys. Rev. B, 41 (1990) 7529-7535.

[23]. L.H. Campbell, PM Fauchet The effects of microcrystal size and shape on the one phonon Raman spectra of crystalline semiconductors. Solid State Communications 58 (1986), 739-741

[24]. B. Lal, S.K. Khosa, R. Tickoo, K.K. Bamzai, P.N. Kotru, Dielectric Characteristics of Melt Grown Doped KMgF3 Crystals. Mater.Chem.& Phys. 83(2004) 158-168.

[25]. D. Ravinder, K. V. Kumar, Dielectric behaviour of erbium substituted Mn–Zn ferrites. Bull. Mater. Sci. 24(2001) 505-509.

[26]. V. Hangloo, R. Tickoo, K.K. Bamzai, P.N. Kotru, Dielectric characteristics of mixed Gd-Ba molybdate crystals grown at ambient temperatures by the gel encapsulation technique. Mater. Chem. Phys. 81(2003) 152-159.

[27] S. Bhat, S.K. Khosa, P.N. Kotru, R.P. Tandon, Dielectric characteristics of gel-grown mixed neodymium-lanthanum-heptamolybdate crystals,. J.Mat.Sci.Lett. 14(1995) 564-567.

[28] A.K Jonscher, A new model of dielectric loss in polymers. Colloid Polym Sci 253(1975) 231–250.

[29]. L.A Dissado, R.M Hill, A Cluster Approach to the Structure of Imperfect Materials and Their Relaxation Spectroscopy. Proc Roy Soc London 390(1983) 131–180.

[30]. L.A. Dissado, R.M. Hill, anomalous low frequency dispersion near direct current conductivity in disordered low dimensional materials. J Chem. Soc. Faraday Trans 80(1984) 291–319.

[31] A.K. Jonscher, The universal dielectric response and its physical significance, IEEE Trans Electron Insul 27(1992) 407–423.

[32]. A.K. Singh, T.C. Goel, R.G. Mendiratta, Dielectric properties of Mn-substituted Ni–Zn ferrites, J Appl Phys 91(2002) 10.

[33]. S.A. Lokare, R.S. Devan, B.K. Chougule, Structural analysis and electrical properties of ME composites. J Alloys Compd 454(2008) 471.

[34]. R.S. Devan, Y.D. Kolekar, B.K. Chougule Magnetoelectric effect and electrical properties in BTO + $Ni_{0.93}Co0.02Cu_{0.05}Fe_2O_4$ particulate composites. J Alloys Compd 461(2008) 678.

[35]. K.K. Patankar, S.S Joshi, B.K. Chougule, Dielectric behaviour in magnetoelectric composites. Phys. Lett A 346(2005) 337.

[36]. D. Adler, J. Feinleib, Electrical and Optical Properties of Narrow-Band Materials. Phys Rev B 2 (1970) 3112.

[37]. V.B. Prasad, R.G. Narsinga, J.W. Chen, B.D. Suresh, Colossal dielectric constant in $PrFeO_3$ semiconductor ceramics, Solid State Sci 14 (2012) 225.

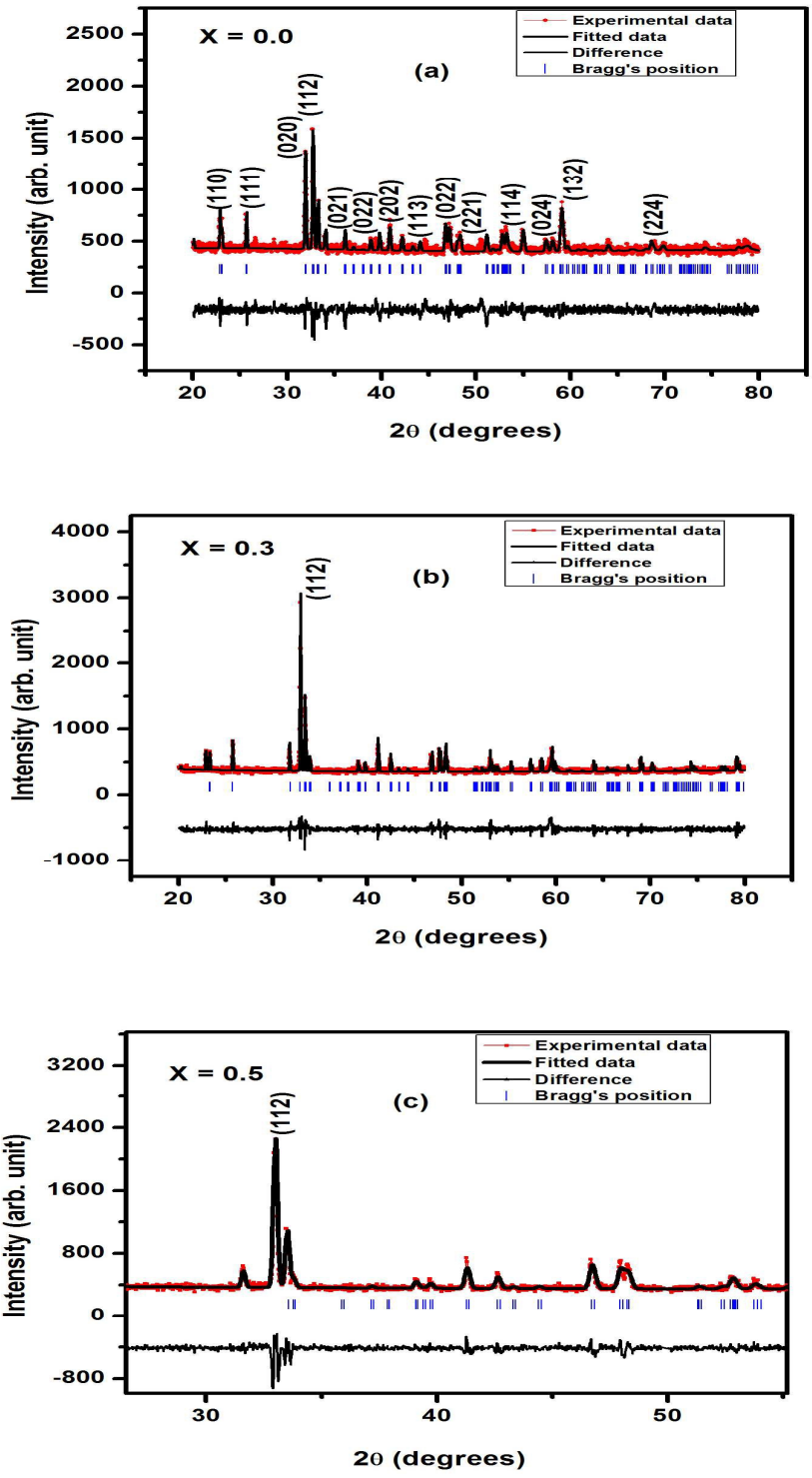

Fig.1. XRD pattern of $EuFe_{1-x}Mn_xO_3$ (x = 0.0, 0.3, 0.5).The structure was investigated by Rietveld treatment of the XRD profiles.

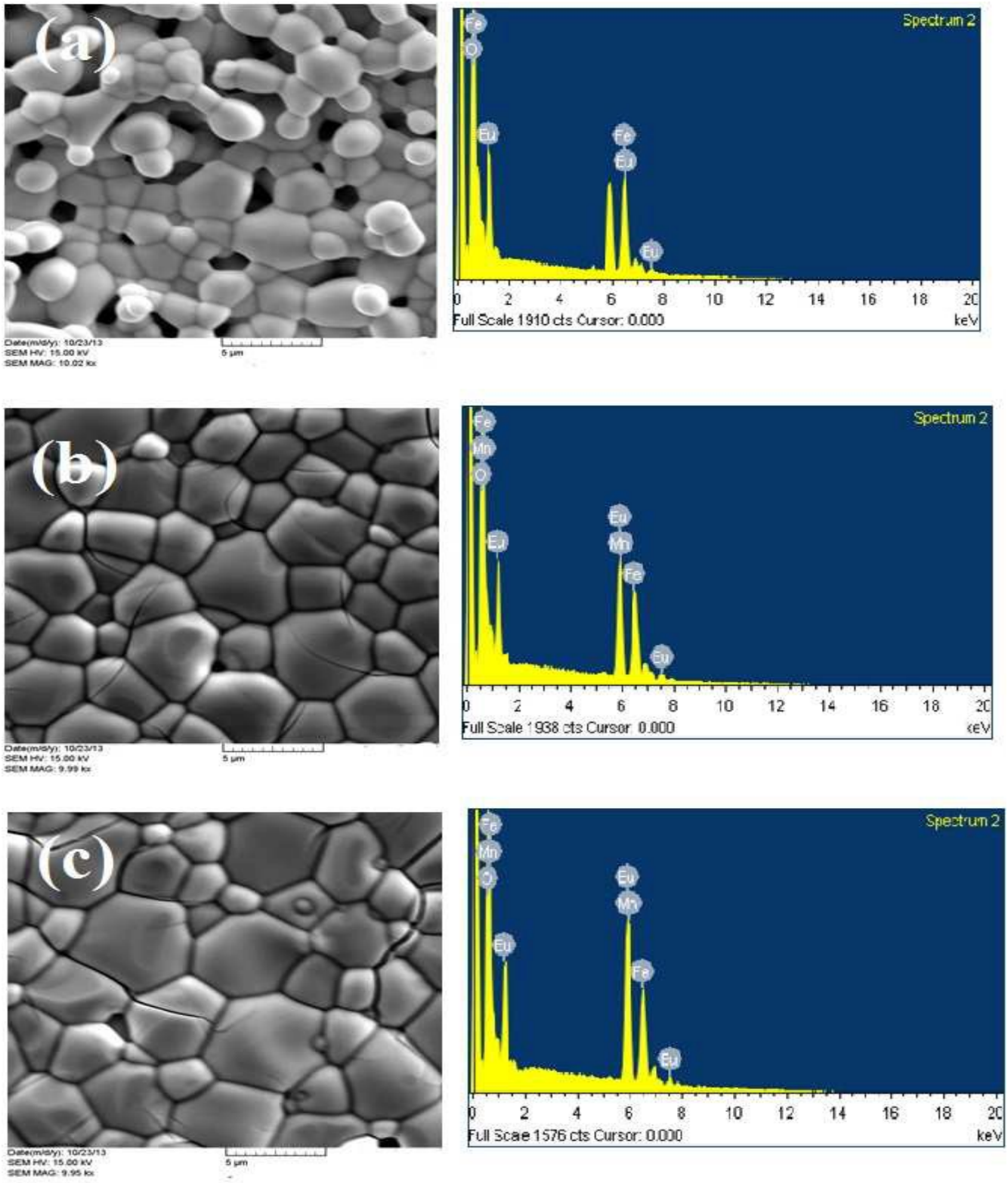

Fig.2. The SEM images along with EDAX of $EuFe_{1-x}Mn_xO_3$ (x = 0, 0.3 and 0.5) sintered at 1300^0C for 24 h.

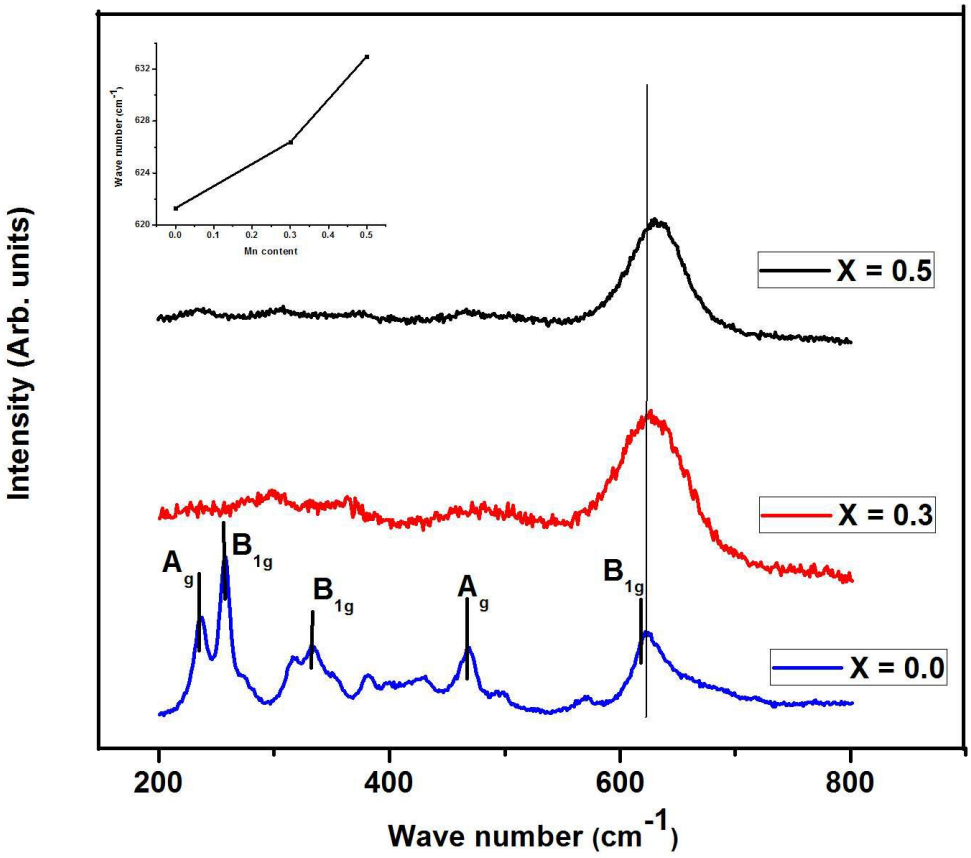

Fig.3. Raman spectra of $EuFe_{1-x}Mn_xO_3$ (x = 0, 0.3 and 0.5). Inset shows shifting of B_{2g} mode to higher wave no. region with doping.

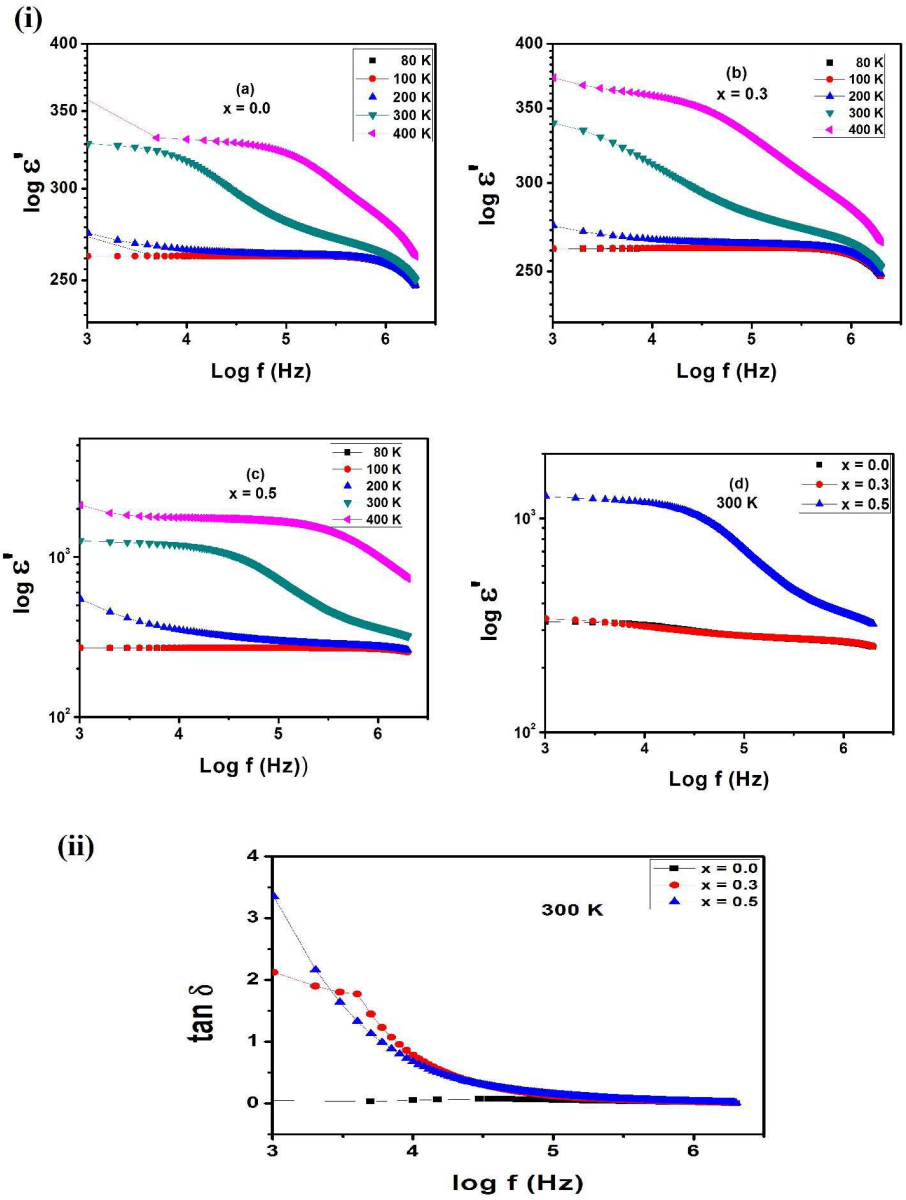

Fig.4. (i) The variation of dielectric constant with frequency of $EuFe_{1-x}Mn_xO_3$ samples for (a) x = 0.0, (b) x = 0.3, (c) x = 0.5, (d) comparative behavior at room temperature.

(ii) Variation of dielectric loss with frequency of $EuFe_{1-x}Mn_xO_3$ samples at room temperature

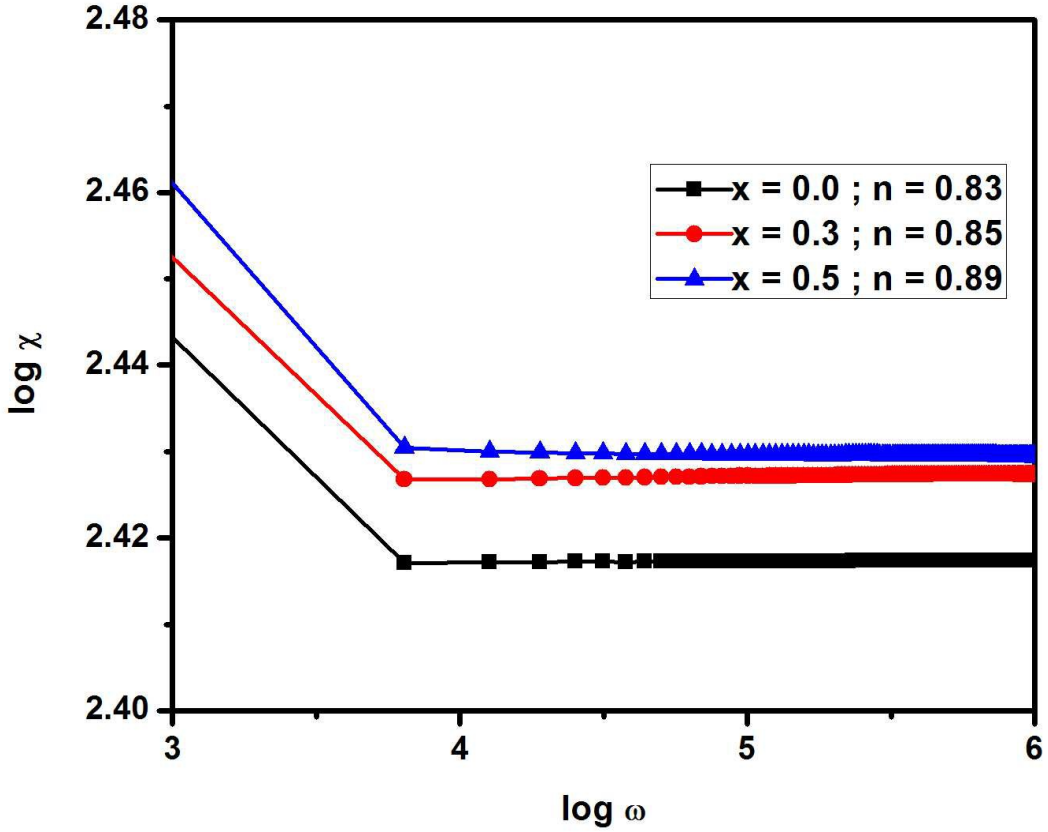

Fig. 5. Variation of logχ verses logω of EFMO compounds.

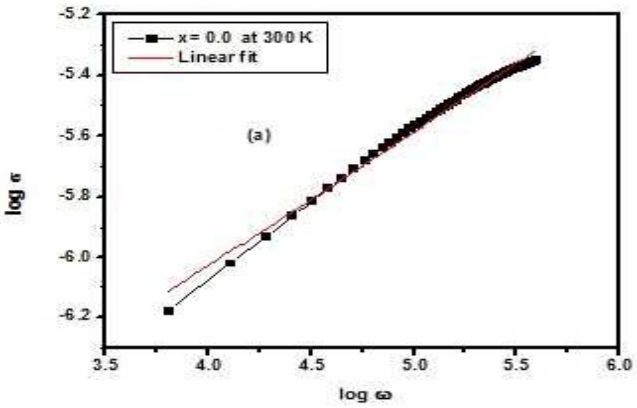

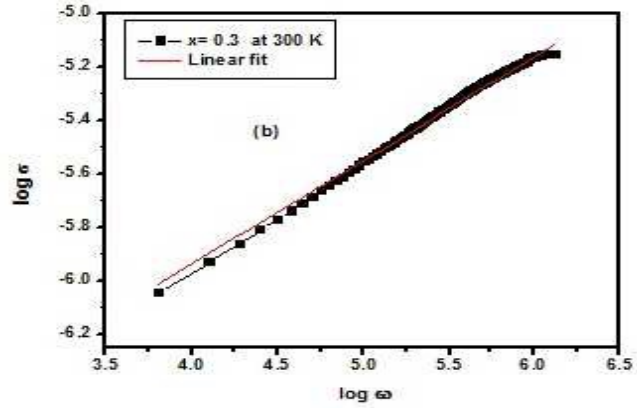

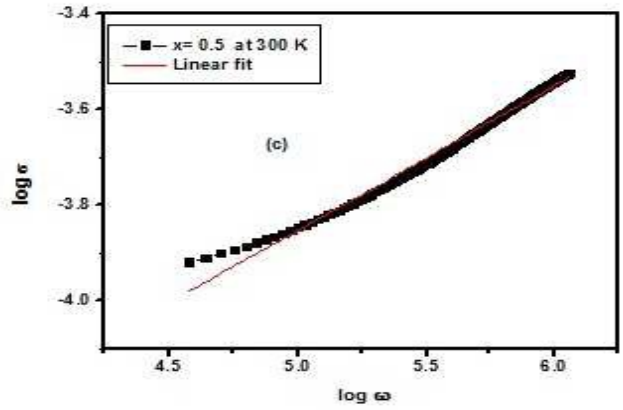

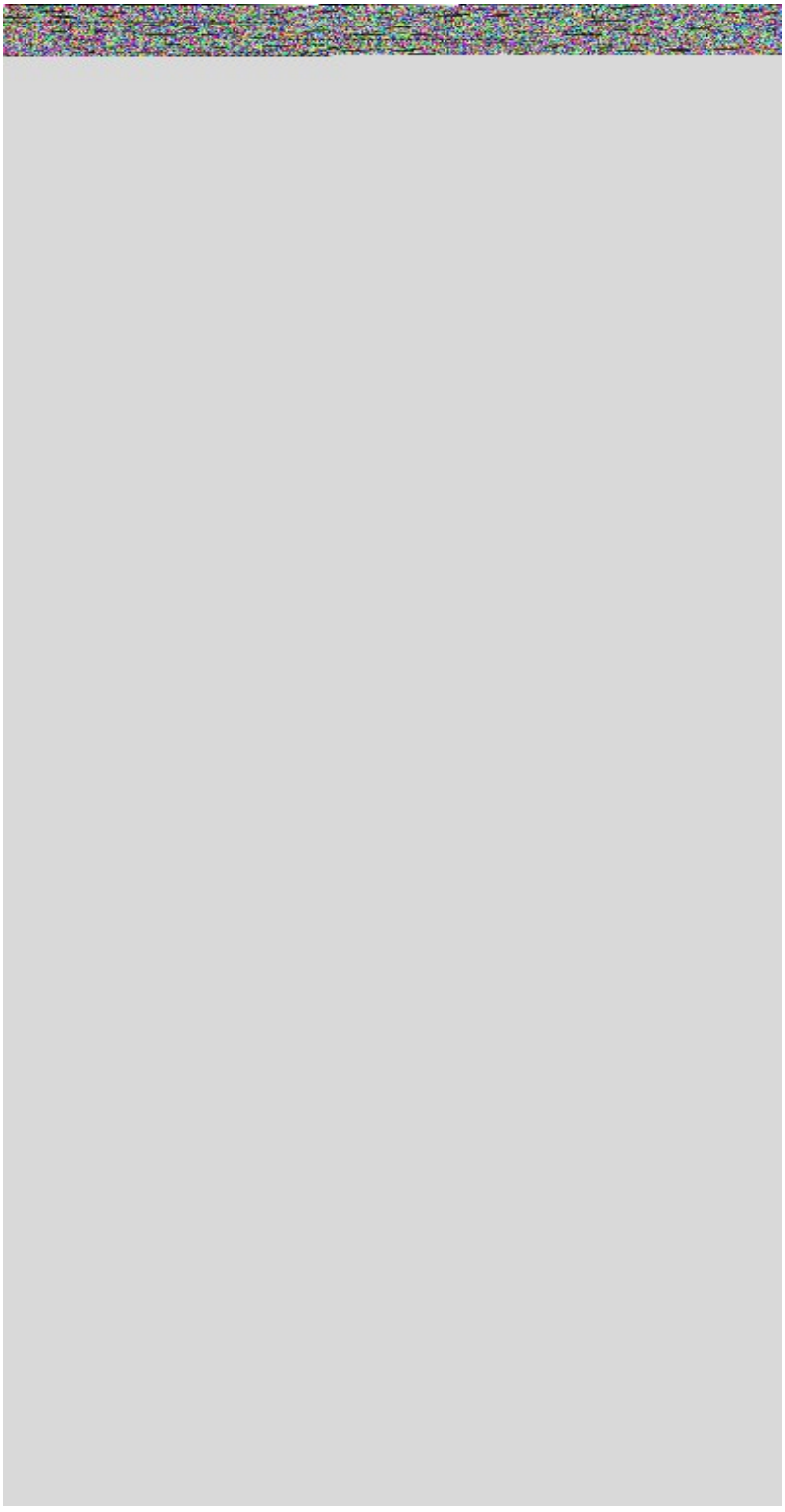

Fig.6. Variation of log σ versus log ω at different composition of EFMO compounds.(a) x = 0.0, (b) x = 0.3, (c) x = 0.5.

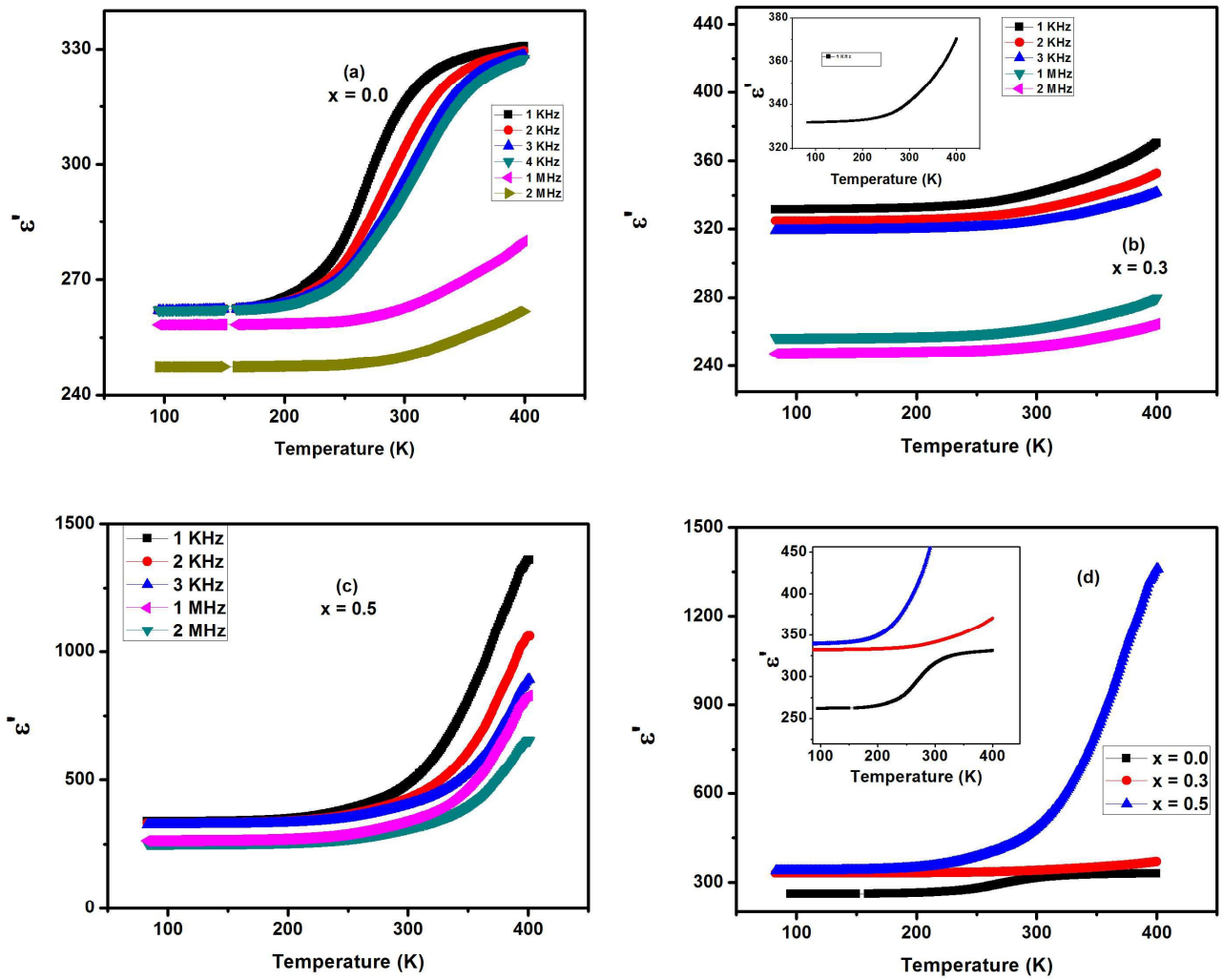

Fig.7. The variation of dielectric constant with temperature at different frequencies of EFMO compounds for (a) x = 0.0, (b) x = 0.3, (c) x = 0.5, (d) comparative behavior at 1 KHz.

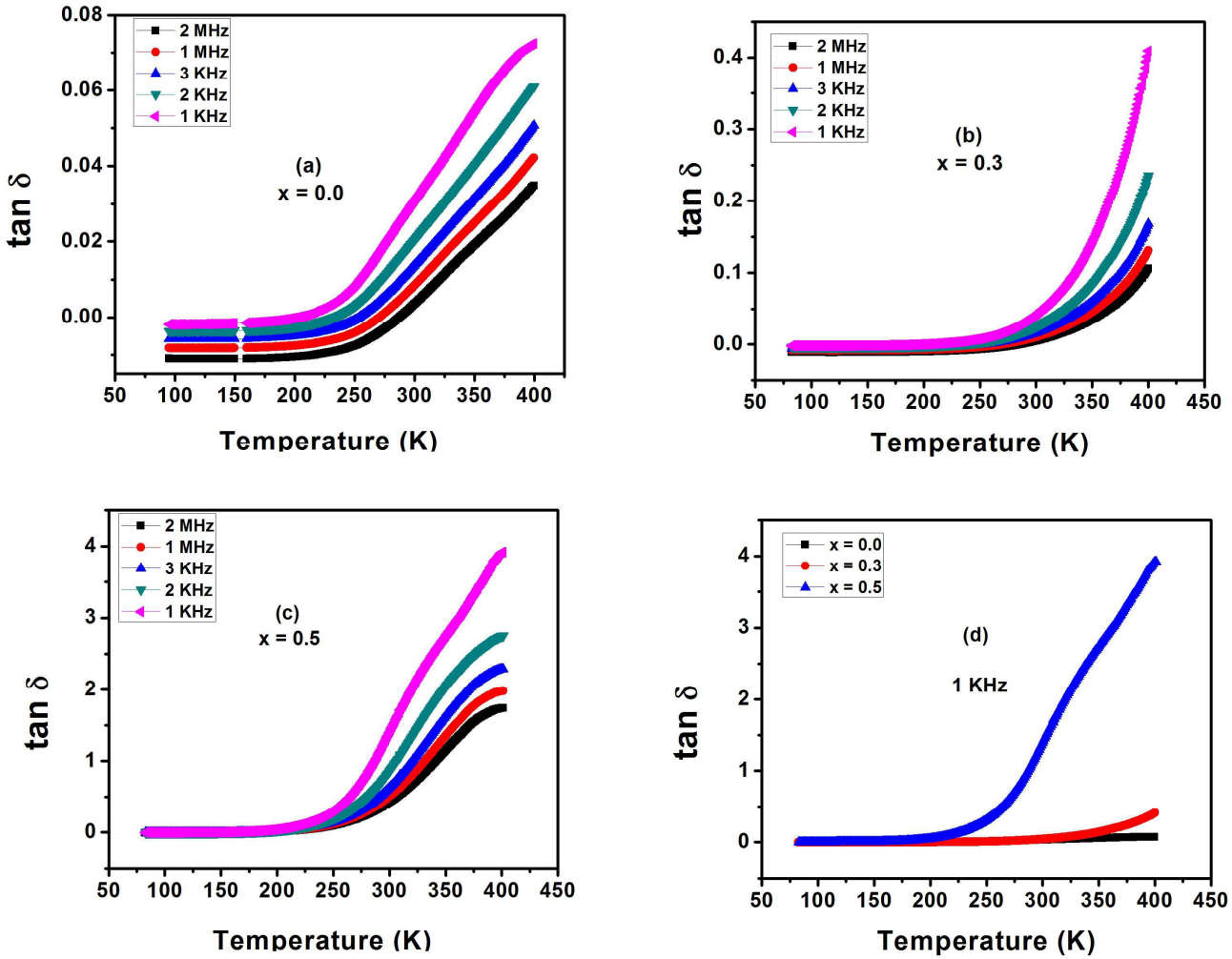

Fig.8. Variation of dielectric loss with temperature at selected frequencies of EFMO compounds for (a) x = 0.0, (b) x = 0.3, (c) x = 0.5, (d) comparative behavior at 1 KHz.

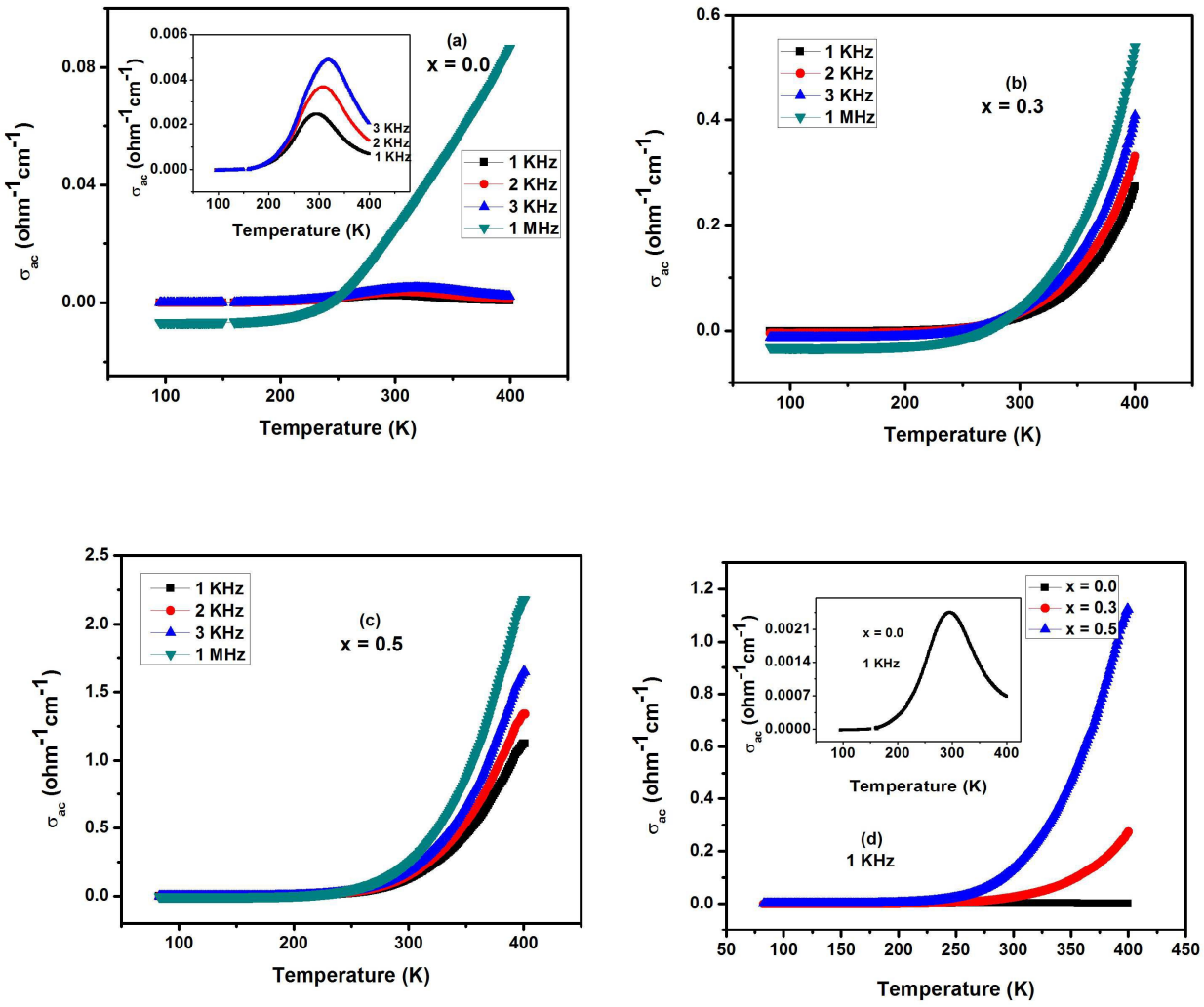

Fig.9. Variation of ac conductivity with temperature at selected frequencies of EFMO compounds for (a) x = 0.0, (b) x = 0.3, (c) x = 0.5, (d) comparative behavior at 1 KHz.

Table-1

The calculated structural parameters and activation energy for different compositions of $EuFe_{1-x}Mn_xO_3$ (x = 0.0, 0.3, 0.5).

Sample	a	b	c	V	χ^2	Rp	Rwp	Rexp	Ea (eV)
x = 0	5.385	5.601	7.702	232.30	2.92	5.69	8.06	4.72	0.23
x = 0.3	5.358	5.629	7.626	230.01	2.78	5.70	8.10	5.05	0.15
x = 0.5	5.345	5.658	7.583	229.31	2.67	5.73	8.56	5.06	0.08

*a, b, c and V are in Å

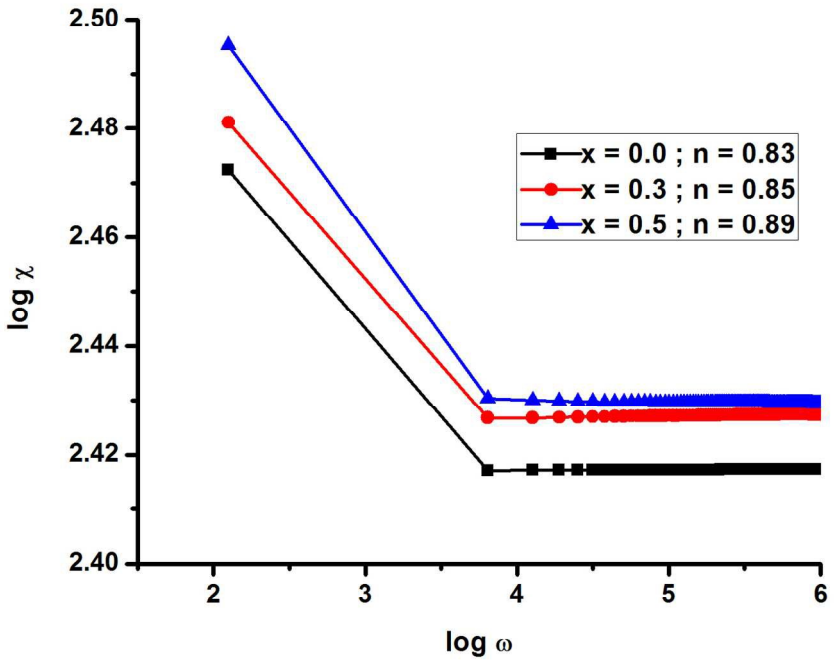

Graphical Abstract
271x206mm (150 x 150 DPI)